Original article

18F-FDG-PET correlates of aging and disease course in ALS as revealed by distinct PVC approaches

Pilar M. Ferraro [a,*], Cristina Campi [b], Alberto Miceli [c,d], Claudia Rolla-Bigliani [a], Matteo Bauckneht [c], Lorenzo Gualco [a,d], Michele Piana [b,e], Cecilia Marini [c,f], Lucio Castellan [a], Silvia Morbelli [c,d], Claudia Caponnetto [g], Gianmario Sambuceti [c,d], Luca Roccatagliata [a,d]

[a] Department of Neuroradiology, IRCCS Ospedale Policlinico San Martino, Largo R. Benzi 10, 16132 Genoa, Italy
[b] LISCOMPlab, Department of Mathematics (DIMA), University of Genoa, Via Balbi 5, 16126 Genoa, Italy
[c] Nuclear Medicine Unit, IRCCS Ospedale Policlinico San Martino, Largo R. Benzi 10, 16132 Genoa, Italy
[d] Department of Health Sciences (DISSAL), University of Genoa, Via Balbi 5, 16126 Genoa, Italy
[e] CNR Superconducting and Other Innovative materials and Devices Institute (SPIN), Corso Ferdinando Maria Perrone 24, 16152 Genoa, Italy
[f] CNR Institute of Molecular Bioimaging and Physiology (IBFM), Via Fratelli Cervi 93, 20054 Segrate, Italy
[g] Department of Neurology, IRCCS Ospedale Policlinico San Martino, Largo R. Benzi 10, 16132 Genoa, Italy

HIGHLIGHTS

- 4 PVC methods were compared to evaluate aging and disease course-related hypometabolism in ALS.
- 3 patterns of significance emerged across ROIs: with all PVC methods, only with MG/SGTM, and only with noPVC/MZ.
- The PVE exerts a significant impact on the detection of metabolism alterations distribution.

GRAPHICAL ABSTRACT
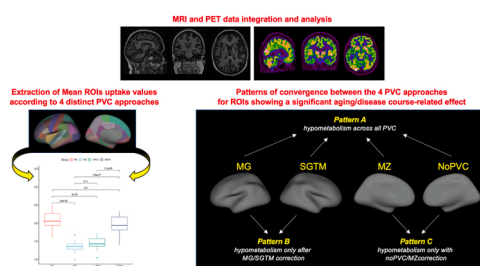
ARTICLE INFO

ABSTRACT

Purpose: The partial volume effect (PVE) complicates PET studies of neurodegenerative diseases, since a decreased 18F-FDG retention might be influenced by atrophy-related changes of cortical regions. Multiple partial volume correction (PVC) methods have been therefore developed, but their application in amyotrophic lateral sclerosis (ALS) is still rare. Additionally, even if metabolic changes have been established in ALS, no study yet has investigated how these may be influenced by aging and disease course. The aim of the present study was therefore to apply and compare multiple PVC approaches to explore aging and disease course-related hypometabolism in ALS.

Methods: PET and MRI data from 15 ALS patients were analyzed using PETSurfer to implement 4 distinct PVC methods: noPVC, Meltzer (MZ), Müller-Gärtner (MG) and Symmetric Geometric Transfer Matrix (SGTM). For each method and Region of Interest (ROI), the 18F-FDG value was regressed against subject age and disease duration.

Abbreviations: ALS, Amyotrophic Lateral Sclerosis; CT, Cortical Thickness; 18F-FDG, 18F Fluorodeoxyglucose; MG, Müller-Gärtner; MZ, Meltzer; PVC, Partial Volume Correction; PVE, Partial Volume Effect; ROI, Region of Interest; SGTM, Symmetric Geometric Transfer Matrix.

* Corresponding author.

E-mail address: PilarMaria.Ferraro@ext.unige.it (P.M. Ferraro).

Results: MG/SGTM application almost halved the number of regions showing a significant age-related hypometabolism, while the same effect was not observed for disease course, where only the distribution of identified regions varied. Three distinct patterns emerged: regions showing a significant age/disease course-related effect across all the different methods, regions yielding significance only with MG/SGTM application, and regions maintaining significance only with noPVC/MZ application.

Conclusions: Significant changes in the distribution of aging and disease course-related hypometabolism were observed when the effect of the underlying structural status was considered, supporting the need for investigate the impact of PVE on PET-assessed metabolic changes in clinical and research settings.

1. Introduction

Accurate brain metabolism estimation in Positron Emission Tomography (PET) studies is often hindered by the partial volume effect (PVE) in which limited scanner resolution causes the activity to appear to spill out of one region and into another [1]. In particular, the PVE effect implies that the intensity of a particular voxel, being related to the size of the emitting source, reflects the tracer concentration not only of the tissue within that voxel but also of the surrounding area [2], complicating metabolism quantification in a specific region due to the loss of its own signal and contamination from adjacent areas.

The PVE is greater in presence of cortical atrophy, since a decreased retention of Fluorodeoxyglucose (^{18}F) (^{18}F-FDG) might either reflect an altered metabolism or simply derive from the atrophy-related changes in size/shape of cortical regions [1].

To overcome this limitation, recent studies are now applying different partial volume correction (PVC) methods to reliably explore metabolism in neurodegenerative diseases such as Alzheimer's disease [3–6] and Mild Cognitive Impairment [7–9], and in normal aging [10–13]. Currently, the most adopted approaches are Meltzer (MZ) [14], Müller-Gärtner (MG) [15], and the Symmetric Geometric Transfer Matrix (SGTM) [16].

Comparing these approaches relative to noPVC analysis in healthy subjects, Greve and colleagues recently found that noPVC had a significant atrophy-induced bias that exaggerated the effect of aging on hypometabolism and was similar to the MZ approach, while MG and SGTM revealed more selective patterns of hypometabolism [1].

In Amyotrophic Lateral Sclerosis (ALS), a fatal neurodegenerative disease with relentless progression, multiple studies reported distinct patterns of metabolism changes [17–20]. However, only few of them have applied any PVC approach to account for the atrophy frequently observed in this condition [21] and none yet has compared the effects of distinct PVC methods application.

Additionally, even if metabolic changes have been established in ALS, no study yet has investigated how these may be influenced by aging and disease course.

In this study we therefore aimed at exploring both aging and disease course-related metabolic alterations in ALS by applying and comparing 4 distinct PVC approaches: noPVC, MZ, MG and SGTM.

Specifically, we hypothesized that, as previously observed in healthy subjects [1], the application of SGTM and MG, by removing the atrophy-induced bias, would have revealed more selective patterns of aging and disease course-related hypometabolism in ALS.

2. Materials and methods

2.1. Subjects

As part of a larger study established at our Institution, all the ALS patients recruited between January 2016 and January 2021 with both PET and MRI scans acquired within a maximum interval of 30 days were included in the present study.

Written informed consent was obtained from each participant according to the Institution's procedures and the Declaration of Helsinki. The study was approved by the Hospital Review Board.

Inclusion criteria were: (1) a diagnosis of possible, probable or definite ALS according to revised El Escorial criteria [22]; and (2) complete clinical characterization and evaluation, including: time and site of symptom onset (bulbar or spinal), age at symptom onset, the ALS functional rating scale revised (ALSFRS-r) [23] and the clinical progression rate estimation (computed with the formula (48-ALFRS-r score at the time of the evaluation) / disease duration at the time of the evaluation).

2.2. PET and MRI integration and analyses

All the details of the PET and MRI acquisition protocols are provided in the Supplementary materials.

T1-weighted MRI images were analyzed using FreeSurfer version 7.1.1. (surfer.nmr.mgh.harvard.edu) [24]. For each of the 68 regions of interest (ROIs) defined according to the Desikan parcellation atlas the following structural metrics were obtained: volume, surface area and cortical thickness (CT).

The PETSurfer tool within Freesurfer 7.1.1 was then used to integrate and analyze PET and MRI data [1,25]. To perform PVC, a high-resolution segmentation was created from the T1-weighted MRI images. PET volumes were registered to the MRI ones using Boundary-based Registration (BBR) by means of a 6 degree of freedom linear transform.

The MRI segmentation was mapped into the PET space in a way that accounted for the tissue fraction effect (TFE) [26], a type of PVE that occurs when multiple tissue types or ROIs occupy the same PET voxel.

PET data were then analyzed using 4 PVC methods: noPVC, MZ, MG and SGTM. In all methods, the ^{18}F-FDG data were reduced to 68 uptake values (one for each ROI according to the Desikan parcellation atlas). All methods used the same PET-MRI registration, segmentation, and point spread function (PSF) and accounted for 3D PVEs. A relative standard uptake value (rSUV) was computed by dividing the ROI intensity by the intensity of pons for the given method. All the methodological details of the analyses performed according to the 4 implemented methods are provided in the Supplementary Materials.

2.3. Statistical analyses

All data were analyzed using CRAN R Version 3.4.1. For each ROI the mean uptake values obtained from the 4 PVC methods were compared between each other using one-way ANOVA with Bonferroni correction for multiple comparisons.

Linear regression models were then used to identify cortical regions in which greater age and disease duration were significantly associated with reduced mean uptake values as estimated using the 4 different PVC methods and structural MRI metrics derived from Freesurfer. For all the analyses the statistical significance threshold was set to $p < 0.05$.

3. Results

3.1. Patient characteristics

Out of the total sample of ALS patients with available MRI and PET scans (N = 16), 1 case was excluded due to motion artefacts on MRI. The

final sample consisted of 15 ALS patients (9 males, 6 females) with a mean age of 61.53 years ($\pm$ 14.54) (Table 1).

3.2. Mean uptake values derived from the different PVC methods

In terms of values ranges, across almost all the ROIs noPVC and MZ resulted in similar mean uptake values, which in turn were significantly lower compared to the ones obtained with MG and SGTM (Table 2).

3.3. Aging and disease course-related metabolic reductions according to the different PVC methods

Both aging and disease duration were associated with metabolism reductions across all the ROIs.

By applying distinct PVC methods, we were able to identify 3 distinct patterns: (1) *"pattern A"*: regions showing a significant age/disease duration-related effect across all the different PVC methods, (2) *"pattern B"*: regions yielding significance for an age/disease duration-related effect only when SGTM/MG corrections were applied, and (3) *"pattern C"*: regions maintaining significance for an age/disease duration-related effect only when noPVC and MZ were used.

3.3.1. Aging effect

Overall, significant associations between aging and reduced metabolism were observed in 15 ROIs (p < 0.05). Twelve ROIs were identified when noPVC was applied, 14 ROIs when MZ was used, while MG and SGTM application yielded the lowest number of significant ROIs (8 and 7, respectively).

Seven ROIs showed *pattern A* (Fig. 1), namely: left temporal pole, right temporal pole, left rostral anterior cingulate, right rostral anterior cingulate, right caudal anterior cingulate, left insula and right insula. One ROI, the left caudal anterior cingulate, showed *pattern B* (Fig. 1).

Seven ROIs showed *pattern C* (Fig. 1), and in particular: left superior temporal, left transverse temporal, left lingual, left cuneus, left pericalcarine, right cuneus and right pericalcarine.

3.3.2. Disease duration effect

Overall, significant associations between disease duration and reduced metabolism were observed in 24 ROIs (p < 0.05). The total number of ROIs identified using the different methods was the same (15 ROIs).

Nine ROIs showed *pattern A* (Fig. 2), namely: left caudal middle frontal, left pars opercularis, left pars triangularis, left lateral orbitofrontal, right pars opercularis, right lateral orbitofrontal, right medial orbitofrontal, right banks of the superior temporal sulcus and right insula.

Eight ROIs showed *pattern B* (Fig. 2), and in particular: right caudal middle frontal, left inferior parietal, right fusiform, left lateral occipital, right lateral occipital, right lingual, left isthmus cingulate and right posterior cingulate.

Seven ROIs showed *pattern C* (Fig. 2), namely: left medial

Table 1
Demographic and clinical features of ALS patients.

ALS sample	
N	15
Gender [F/M]	6/9
Age [years]	61.53 $\pm$ 14.54
Site of onset [spinal/bulbar]	13/2
Disease duration [months]	9.20 $\pm$ 3.27
ALFRS-r [0–48]	41.41 $\pm$ 3.87
Rate of progression [points/month]	0.87 $\pm$ 0.81
Interval between PET and MRI exams [days]	8.00 $\pm$ 6.81

Note. Values are means $\pm$ standard deviations or frequencies. Abbreviations. ALSFRS-r = ALS functional rating scale revised; F= females; M= males; MRI= Magnetic Resonance Imaging; PET= Positron Emission Tomography.

orbitofrontal, left banks of the superior temporal sulcus, left transverse temporal, right transverse temporal, left pericalcarine, right rostral anterior cingulate and left insula.

3.4. Aging and disease course-related structural reductions

Significant associations between aging and reduced structural metrics were observed in 19 ROIs (p < 0.05) (Fig. 1), and in particular: CT reductions in the left transverse temporal; volume reductions in the left pars opercularis, left pars triangularis, left paracentral, left middle temporal, left inferior temporal, left entorhinal, right rostral middle frontal, right paracentral, left inferior parietal, right inferior parietal, right postcentral, right superior temporal, right middle temporal, right pars triangularis, and right transverse temporal; volume and surface area reductions in the left lateral occipital and right lateral orbitofrontal; surface area reductions in the right posterior cingulate. Conversely, none of the ROIs showed significant disease duration-related structural reductions.

4. Discussion

To our knowledge, this is the first study comparing different PVC approaches to explore aging and disease course-related hypometabolism in ALS.

We found that MZ and noPVC resulted in similar mean uptake values, which in turn were significantly lower compared to the ones obtained with MG and SGTM approaches.

The dichotomy between MG/SGTM and MZ/noPVC was further confirmed by the regression analyses results, in which *pattern B* and *pattern C* were identified.

These results are in line with the previous study from Greve and coworkers, who found that MZ was almost the same as noPVC for liberal brain masks, while MG and SGTM were similar between each other [1].

When we looked at the effect of aging on metabolism, more regions were identified when noPVC/MZ were used, while the application of MG/SGTM almost halved the number of regions showing a significant association. Again, this finding is in accordance with the results obtained from Greve and colleagues, confirming that noPVC leads to a significant atrophy-induced bias that exaggerates the effect of age on hypometabolism [1].

These observations are not surprising given the previously reported effect of aging on atrophy in both healthy subjects [27] and ALS patients [28], but provide important evidence for supporting the use of PVC in PET studies.

Notably, when we looked at the effects of disease course on metabolism, we did not observe the same pattern since the number of identified ROIs was stable across all the different PVC corrections. This finding suggests that, differently from aging, disease course in ALS may initially have a greater impact on neuronal activity rather than on structure. Accordingly, we did not observe any significant disease course-related structural reduction in our study.

Relative to other neurodegenerative diseases such as Alzheimer's disease and frontotemporal dementia, indeed, the effect of progressing pathology on grey matter structural reductions in ALS has been less consistently suggested. While few previous studies have reported progressive cortical atrophy in ALS [29,30], more recent observations suggest that functional alterations may predate structural involvement [31,32].

Notably, by applying multiple PVC approaches we were able to identify 3 distinct patterns of results.

Regions in *pattern A* were the ones remaining stable across all the different PVC methods. We interpreted this pattern as the one characterizing regions in which metabolic reductions were so severe to be evident independently from the underlying structural status. Accordingly, while some of them also showed structural reductions related to aging, others did not.

Table 2

Mean uptake values in the 68 ROIs of the Desikan parcellation scheme as obtained using the four different implemented methods.

	Left Hemisphere				Right Hemisphere			
	NoPVC	MZ	MG	SGTM	NoPVC	MZ	MG	SGTM
Superior frontal	1.72 ± 0.18*	1.61 ± 0.19*	2.67 ± 0.25[a,d]	2.70 ± 0.27[a,d]	1.72 ± 0.18[b,c]	1.61 ± 0.19[b,c]	2.68 ± 0.24[a,d]	2.70 ± 0.26[a,d]
Rostral middle frontal	1.86 ± 0.24*	1.70 ± 0.23*	2.90 ± 0.37[a,d]	2.94 ± 0.39[a,d]	1.84 ± 0.24*	1.70 ± 0.23*	2.85 ± 0.35[a,d]	2.89 ± 0.37[a,d]
Caudal middle frontal	1.96 ± 0.22*	1.79 ± 0.23*	3.19 ± 0.33[a,d]	3.34 ± 0.41[a,d]	1.92 ± 0.21*	1.76 ± 0.21*	3.08 ± 0.28[a,d]	3.19 ± 0.31[a,d]
Pars opercularis	1.85 ± 0.26*	1.68 ± 0.25*	2.87 ± 0.36[a,d]	2.98 ± 0.40[a,d]	1.85 ± 0.24*	1.69 ± 0.22*	2.79 ± 0.31[a,d]	2.89 ± 0.36[a,d]
Pars orbitalis	1.73 ± 0.25*	1.62 ± 0.25*	2.72 ± 0.42[a,d]	2.75 ± 0.46[a,d]	1.76 ± 0.25*	1.66 ± 0.25*	2.70 ± 0.39[a,d]	2.75 ± 0.43[a,d]
Pars triangularis	1.80 ± 0.25[b,c]	1.66 ± 0.2*	2.83 ± 0.39[a,d]	2.91 ± 0.45[a,d]	1.80 ± 0.24*	1.68 ± 0.24[b,c]	2.78 ± 0.36[a,d]	2.85 ± 0.38[a,d]
Lateral orbitofrontal	1.66 ± 0.16*	1.55 ± 0.17*	2.51 ± 0.28[a,d]	2.58 ± 0.30[a,d]	1.66 ± 0.15[b,c]	1.55 ± 0.16[b,c]	2.48 ± 0.28[a,d]	2.56 ± 0.31[a,d]
Medial orbitofrontal	1.58 ± 0.18[b,c]	1.47 ± 0.17[b,c]	2.27 ± 0.26[a,d]	2.30 ± 0.28[a,d]	1.62 ± 0.17*	1.50 ± 0.17*	2.30 ± 0.26[a,d]	2.34 ± 0.27[a,d]
Precentral	1.71 ± 0.13*	1.58 ± 0.16*	2.90 ± 0.20[a,d]	2.93 ± 0.21[a,d]	1.70 ± 0.14*	1.58 ± 0.17*	2.84 ± 0.23[a,d]	2.86 ± 0.24[a,d]
Paracentral	1.66 ± 0.20*	1.52 ± 0.19*	2.73 ± 0.36[a,d]	2.71 ± 0.44[a,d]	1.67 ± 0.18*	1.53 ± 0.18*	2.72 ± 0.32[a,d]	2.74 ± 0.42[a,d]
Frontal pole	1.58 ± 0.21[b,c]	1.53 ± 0.21[b,c]	2.55 ± 0.33[a,d]	2.61 ± 0.37[a,d]	1.63 ± 0.20[b,c]	1.56 ± 0.20[b,c]	2.62 ± 0.33[a,d]	2.71 ± 0.38[a,d]
Superior parietal	1.63 ± 0.19[b,c]	1.53 ± 0.19[b,c]	2.72 ± 0.30[a,d]	2.76 ± 0.33[a,d]	1.61 ± 0.20[b,c]	1.51 ± 0.20[b,c]	2.69 ± 0.33[a,d]	2.72 ± 0.36[a,d]
Inferior parietal	1.72 ± 0.22*	1.60 ± 0.22*	2.60 ± 0.33[a,d]	2.62 ± 0.36[a,d]	1.71 ± 0.20[b,c]	1.60 ± 0.20[b,c]	2.55 ± 0.28[a,d]	2.57 ± 0.30[a,d]
Supramarginal	1.67 ± 0.17*	1.55 ± 0.19*	2.57 ± 0.25[a,d]	2.62 ± 0.26[a,d]	1.62 ± 0.14*	1.52 ± 0.15*	2.48 ± 0.22[a,d]	2.50 ± 0.24[a,d]
Postcentral	1.65 ± 0.15*	1.52 ± 0.17*	2.86 ± 0.23[a,d]	2.90 ± 0.26[a,d]	1.66 ± 0.15*	1.53 ± 0.16*	2.83 ± 0.26[a,d]	2.89 ± 0.29[a,d]
Precuneus	1.98 ± 0.27*	1.77 ± 0.25*	2.97 ± 0.42[a,d]	3.05 ± 0.47[a,d]	1.95 ± 0.24*	1.75 ± 0.23*	2.93 ± 0.41[a,d]	2.99 ± 0.41[a,d]
Superior temporal	1.44 ± 0.17[b,c]	1.37 ± 0.17[b,c]	2.14 ± 0.21[a,d]	2.06 ± 0.21[a,d]	1.45 ± 0.15[b,c]	1.39 ± 0.16[b,c]	2.12 ± 0.19[a,d]	2.05 ± 0.19[a,d]
Middle temporal	1.57 ± 0.18[b,c]	1.48 ± 0.18[b,c]	2.23 ± 0.24[a,d]	2.26 ± 0.25[a,d]	1.56 ± 0.17[b,c]	1.49 ± 0.17[b,c]	2.18 ± 0.22[a,d]	2.19 ± 0.23[a,d]
Inferior temporal	1.49 ± 0.17[b,c]	1.42 ± 0.18[b,c]	2.09 ± 0.24[a,d]	2.08 ± 0.26[a,d]	1.46 ± 0.16[b,c]	1.41 ± 0.17[b,c]	2.05 ± 0.21[a,d]	2.03 ± 0.24[a,d]
Banks of the superior temporal sulcus	1.72 ± 0.15*	1.56 ± 0.16*	2.41 ± 0.17[a,d]	2.51 ± 0.18[a,d]	1.73 ± 0.15*	1.58 ± 0.13*	2.35 ± 0.20[a,d]	2.43 ± 0.21[a,d]
Fusiform	1.47 ± 0.11[b,c]	1.39 ± 0.13[b,c]	1.96 ± 0.19[a,d]	1.92 ± 0.19[a,d]	1.46 ± 0.10*	1.37 ± 0.12*	1.92 ± 0.16[a,d]	1.86 ± 0.16[a,d]
Transverse temporal	2.04 ± 0.32*	1.76 ± 0.29*	3.10 ± 0.35*	3.91 ± 0.54*	2.04 ± 0.31*	1.75 ± 0.27*	3.06 ± 0.41*	4.04 ± 0.72*
Entorhinal	1.06 ± 0.17[b,c]	1.08 ± 0.15[b,c]	1.52 ± 0.24[a,d]	1.46 ± 0.25[a,d]	1.07 ± 0.16[b,c]	1.08 ± 0.15[b,c]	1.54 ± 0.26[a,d]	1.49 ± 0.28[a,d]
Temporal pole	1.06 ± 0.10[b,c]	1.08 ± 0.11[b,c]	1.48 ± 0.15*	1.36 ± 0.16*	1.07 ± 0.11[b,c]	1.08 ± 0.09[b,c]	1.49 ± 0.14*	1.36 ± 0.17*
Parahippocampal	1.18 ± 0.13[b,c]	1.15 ± 0.12[b,c]	1.63 ± 0.25[a,d]	1.53 ± 0.28[a,d]	1.19 ± 0.10[b,c]	1.16 ± 0.10[b,c]	1.63 ± 0.18[a,d]	1.52 ± 0.23[a,d]
Lateral occipital	1.64 ± 0.23[b,c]	1.54 ± 0.22[b,c]	2.64 ± 0.40[a,d]	2.67 ± 0.43[a,d]	1.63 ± 0.19[b,c]	1.54 ± 0.19[b,c]	2.58 ± 0.33[a,d]	2.59 ± 0.33[a,d]
Lingual	1.76 ± 0.24[b,c]	1.58 ± 0.24[b,c]	2.60 ± 0.37[a,d]	2.64 ± 0.37[a,d]	1.78 ± 0.27[b,c]	1.60 ± 0.24[b,c]	2.64 ± 0.48[a,d]	2.68 ± 0.53[a,d]
Cuneus	2.03 ± 0.31*	1.76 ± 0.29*	3.18 ± 0.51[a,d]	3.31 ± 0.60[a,d]	2.00 ± 0.37[b,c]	1.75 ± 0.31[b,c]	3.14 ± 0.66[a,d]	3.24 ± 0.77[a,d]
Pericalcarine	2.23 ± 0.35*	1.86 ± 0.29*	3.65 ± 0.68*	4.24 ± 0.89*	2.28 ± 0.41*	1.91 ± 0.33*	3.63 ± 0.77*	4.17 ± 0.97*
Rostral anterior cingulate	1.52 ± 0.16[b,c]	1.42 ± 0.15[b,c]	2.08 ± 0.22[a,d]	2.01 ± 0.25[a,d]	1.46 ± 0.12[b,c]	1.37 ± 0.13[b,c]	2.01 ± 0.19*	1.84 ± 0.18*
Caudal anterior cingulate	1.44 ± 0.18[b,c]	1.35 ± 0.16[b,c]	2.10 ± 0.24[a,d]	1.97 ± 0.27[a,d]	1.42 ± 0.16[b,c]	1.34 ± 0.15[b,c]	2.10 ± 0.23[a,d]	1.98 ± 0.28[a,d]
Posterior cingulate	1.83 ± 0.20*	1.64 ± 0.21*	2.69 ± 0.33[a,d]	2.70 ± 0.32[a,d]	1.81 ± 0.22*	1.63 ± 0.22*	2.63 ± 0.33[a,d]	2.63 ± 0.36[a,d]
Isthmus cingulate	1.77 ± 0.26*	1.61 ± 0.24*	2.66 ± 0.39[a,d]	2.69 ± 0.45[a,d]	1.78 ± 0.29*	1.62 ± 0.26*	2.67 ± 0.46[a,d]	2.71 ± 0.53[a,d]
Insula	1.41 ± 0.14[b,c]	1.34 ± 0.14[b,c]	1.97 ± 0.20*	1.76 ± 0.19*	1.44 ± 0.14[b,c]	1.36 ± 0.15[b,c]	1.98 ± 0.20*	1.80 ± 0.18*

Note. Values are means ± standard deviations. [a] $p < 0.05$ compared to MZ; [b] $p < 0.05$ compared to MG; [c] $p < 0.05$ compared to SGTM; [d] $p < 0.05$ compared to noPVC; * $p < 0.05$ compared to all other methods. Abbreviations. MG= Müller-Gärtner; MZ= Meltzer; PVC= partial volume correction; SGTM= Symmetric Geometric Transfer Matrix.
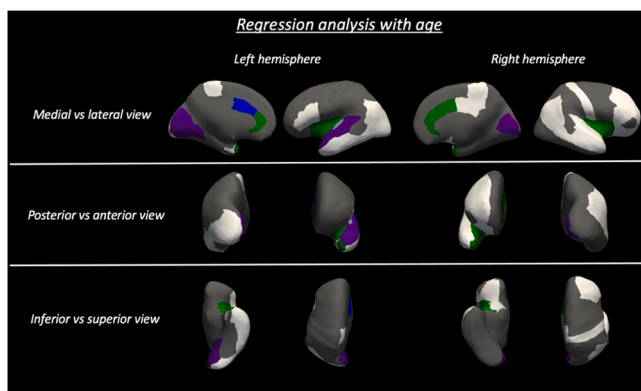

Fig. 1. Regions of Interest (ROIs) showing a significant age-related effect. Regions in *pattern A* are shown in green, regions in *pattern B* are shown in blue, regions in *pattern C* are shown in purple, regions showing selective structural reductions are shown in white, regions with overlapping *pattern C* and structural reductions (only the left transverse temporal region) are shown in light purple.

Fig. 2. Regions of Interest (ROIs) showing a significant disease course-related effect. Regions in *pattern A* are shown in yellow, regions in *pattern B* are shown in orange, regions in *pattern C* are shown in red.

For the aging analysis, regions in *pattern A* (mainly cingulate areas and insula) were the same identified as stable across different corrections also in the paper by Greve and colleagues [1], further confirming the significant effect of aging on metabolism in these regions. Notably, while this finding has been previously reported in healthy subjects, in the present work we have further widened these observations showing the same effect in a diseased population.
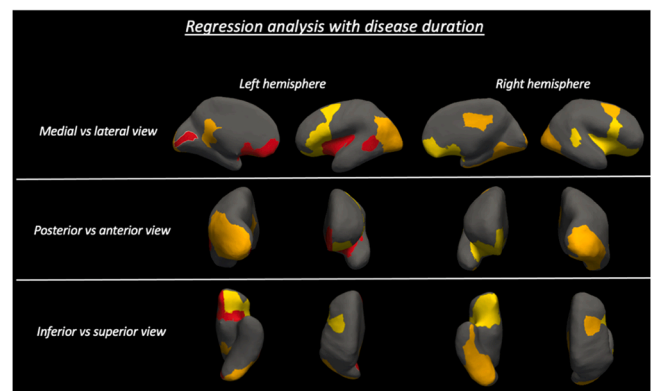
For the disease course analysis, regions in *pattern A* were mainly frontotemporal, in line with the well-known involvement of these regions over disease course [31,33].

Regions in *pattern B* were the ones yielding significance only when MG/SGTM were applied. We interpreted these regions as the ones in which there was still a significant reduction in metabolism considering the relatively preserved structural substrate.

For the aging analysis, only the left caudal anterior cingulate showed

pattern B, and, in line with our hypothesis, there were no age-associated structural reductions in this region.

For the disease course analysis, *pattern B* was mainly observed in parieto-occipital regions, which are generally structurally preserved until advanced disease stages in ALS and, accordingly, no disease course-associated structural reductions were observed in these regions.

It is noteworthy, however, that by applying multiple PVC approaches we were able to reveal that even structurally preserved regions may manifest metabolic reductions, confirming the hypothesis that these may precede structural reductions.

Regions in *pattern C* were those maintaining significance only with noPVC/MZ. We interpreted these regions as the ones in which, removing the possible effect of structural loss, metabolism was not significantly reduced.

For both aging and disease course analyses, however, not all the regions *in pattern C* were showing significant structural reductions, which is due to the previously observed phenomenon that noPVC condition can detect false decreases in metabolism even in structurally preserved regions [1].

We acknowledge that the main limitation of our study is the relatively small sample size. Patients were indeed selected based on the availability of both PET and MRI scans acquired within the same month, which significantly limited the number of eligible cases. Future studies in larger samples are therefore warranted to further widen our findings and ameliorate methodological approaches to the study of the disease.

In particular, given the well-known influence of white matter degeneration on cortical functional activity, future efforts should be focused on generating improved segmentation procedures to separately estimate grey and white matter metabolism alterations, and promising advances in the field are already available.

The PMOD software has been recently used to assess white matter glucose metabolism in patients with Alzheimer's disease [34]. After generating grey and white matter binary masks, the software uses probability atlases to obtain an accurate labeling of distinct areas within both tissue types, enabling to separately quantify grey and white matter specific binding ratios.

Another promising approach is the Generative adversarial network (GAN) which has proved to be a powerful tool for automatically segmenting and estimating volumes of white matter hyperintensities on ^{18}F-FDG PET/CT images [35], paving the way towards tissue-specific approaches to the study of brain metabolism alterations.

As increasingly outlined, however, reliable estimation of white matter metabolism is further complicated by the PVE, which reduces apparent ^{18}F-FDG uptake levels in high-uptake regions (such as grey matter) and increases apparent uptake levels in adjacent low-uptake regions (such as white matter). In this context, new voxel-based PVC methods for quantifying physiological white matter uptake, such as the Local Regression Analysis (LoReAn) algorithm, have been developed and validated against the GTM approach, showing an improvement of both bias and variations coefficient in white matter regions [36].

While looking ahead to the increasing application of these methodological advances, this is the first study, to our knowledge, comparing different PVC approaches to evaluate aging and disease course-related hypometabolism in ALS.

While we observed widespread extra-motor metabolic reductions related to these processes, we also unraveled significant changes in their regional distribution when the effect of the underlying structural status was considered. The heterogeneity of the results we obtained using different PVC corrections might provide a valuable explanation for the diversity of findings from previous studies investigating metabolism alterations in neurodegenerative diseases and suggests that the PVC method used highly influences the results obtained and their interpretation.

5. Conclusions

In conclusion, our study provides preliminary evidence supporting the need for systematically investigate the impact of PVE on PET-assessed metabolic changes to improve our fundamental understanding of functional changes associated with ALS pathology.

Ethical Statement

Written informed consent was obtained from each participant according to the Institution's procedures and the Declaration of Helsinki. The study was approved by the Hospital Review Board.

CRediT authorship contribution statement

Pilar M. Ferraro: Conceptualization, Methodology, Formal analysis, Investigation. **Cristina Campi:** Methodology, Formal analysis, Investigation. **Alberto Miceli:** Methodology. **Claudia Rolla-Bigliani:** Methodology. **Matteo Bauckneht:** Methodology. **Lorenzo Gualco:** Methodology. **Michele Piana:** Methodology. **Cecilia Marini:** Formal analysis, Investigation. **Lucio Castellan:** Supervision. **Silvia Morbelli:** Formal analysis, Investigation. **Claudia Caponnetto:** Methodology. **Gianmario Sambuceti:** Conceptualization, Supervision. **Luca Rocca-tagliata:** Conceptualization, Supervision. All authors contributed to manuscript editing and revision and approved the final version.

Declaration of Competing Interest

The authors declare that they have no known competing financial interests or personal relationships that could have appeared to influence the work reported in this paper.

Acknowledgments

Declarations of Interest

none.

Appendix A. Supporting information

Supplementary data associated with this article can be found in the online version at doi:10.1016/j.ejro.2022.100394.

References

[1] D.N. Greve, D.H. Salat, S.L. Bowen, D. Izquierdo-Garcia, A.P. Schultz, C. Catana, J. A. Becker, C. Svarer, G.M. Knudsen, R.A. Sperling, K.A. Johnson, Different partial volume correction methods lead to different conclusions: An 18F-FDG-PET study of aging, Neuroimage (2016), https://doi.org/10.1016/j.neuroimage.2016.02.042.

[2] J. Yang, C. Hu, N. Guo, J. Dutta, L.M. Vaina, K.A. Johnson, J. Sepulcre, G. El Fakhri, Q. Li, Partial volume correction for PET quantification and its impact on brain network in Alzheimer's disease, Sci. Rep. (2017), https://doi.org/10.1038/s41598-017-13339-7.

[3] C.C. Meltzer, J.K. Zubieta, J. Brandt, L.E. Tune, H.S. Mayberg, J.J. Frost, Regional hypometabolism in Alzheimer's disease as measured by positron emission tomography after correction for effects of partial volume averaging, Neurology (1996), https://doi.org/10.1212/WNL.47.2.454.

[4] M. Samuraki, I. Matsunari, W.P. Chen, K. Yajima, D. Yanase, A. Fujikawa, N. Takeda, S. Nishimura, H. Matsuda, M. Yamada, Partial volume effect-corrected FDG PET and grey matter volume loss in patients with mild Alzheimer's disease, Eur. J. Nucl. Med. Mol. Imaging. (2007), https://doi.org/10.1007/s00259-007-0454-x.

[5] G. Chételat, B. Desgranges, B. Landeau, F. Mézenge, J.B. Poline, V. De La Sayette, F. Viader, F. Eustache, J.C. Baron, Direct voxel-based comparison between grey matter hypometabolism and atrophy in Alzheimer's disease, Brain (2008), https://doi.org/10.1093/brain/awm288.

[6] S. Förster, B.H. Yousefi, H.J. Wester, E. Klupp, A. Rominger, H. Förstl, A. Kurz, T. Grimmer, A. Drzezga, Quantitative longitudinal interrelationships between brain

metabolism and amyloid deposition during a 2-year follow-up in patients with early Alzheimer's disease, Eur. J. Nucl. Med. Mol. Imaging. (2012), https://doi.org/10.1007/s00259-012-2230-9.

[7] S.J. Teipel, J. Kurth, B. Krause, M.J. Grothe, The relative importance of imaging markers for the prediction of Alzheimer's disease dementia in mild cognitive impairment - Beyond classical regression, NeuroImage Clin. (2015), https://doi.org/10.1016/j.nicl.2015.05.006.

[8] B.J. Hanseeuw, A.P. Schultz, R.A. Betensky, R.A. Sperling, K.A. Johnson, Decreased hippocampal metabolism in high-amyloid mild cognitive impairment, Alzheimer's Dement (2009), https://doi.org/10.1016/j.jalz.2016.06.2357.

[9] M.D. Paranjpe, X. Chen, M. Liu, I. Paranjpe, J.P. Leal, R. Wang, M.G. Pomper, D. F. Wong, T.L.S. Benzinger, Y. Zhou, The effect of ApoE ε4 on longitudinal brain region-specific glucose metabolism in patients with mild cognitive impairment: a FDG-PET study, NeuroImage Clin. (2019), https://doi.org/10.1016/j.nicl.2019.101795.

[10] D. Yanase, I. Matsunari, K. Yajima, W. Chen, A. Fujikawa, S. Nishimura, H. Matsuda, M. Yamada, Brain FDG PET study of normal aging in Japanese: Effect of atrophy correction, Eur. J. Nucl. Med. Mol. Imaging. (2005), https://doi.org/10.1007/s00259-005-1767-2.

[11] G. Kalpouzos, G. Chételat, J.C. Baron, B. Landeau, K. Mevel, C. Godeau, L. Barré, J. M. Constans, F. Viader, F. Eustache, B. Desgranges, Voxel-based mapping of brain gray matter volume and glucose metabolism profiles in normal aging, Neurobiol. Aging. (2009), https://doi.org/10.1016/j.neurobiolaging.2007.05.019.

[12] P.K. Curiati, J.H. Tamashiro-Duran, F.L.S. Duran, C.A. Buchpiguel, P. Squarzoni, D. C. Romano, H. Vallada, P.R. Menezes, M. Scazufca, G.F. Busatto, T.C.T.F. Alves, Age-related metabolic profiles in cognitively healthy elders: Results from a voxel-based [18F]fluorodeoxyglucose-positron-emission tomography study with partial volume effects correction, Am. J. Neuroradiol. (2011), https://doi.org/10.3174/ajnr.A2321.

[13] D.S. Knopman, C.R. Jack, H.J. Wiste, E.S. Lundt, S.D. Weigand, P. Vemuri, V. J. Lowe, K. Kantarci, J.L. Gunter, M.L. Senjem, M.M. Mielke, R.O. Roberts, B. F. Boeve, R.C. Petersen, 18F-fluorodeoxyglucose positron emission tomography, aging, and apolipoprotein E genotype in cognitively normal persons, Neurobiol. Aging (2014), https://doi.org/10.1016/j.neurobiolaging.2014.03.006.

[14] C.C. Meltzer, P.E. Kinahan, P.J. Greer, T.E. Nichols, C. Comtat, M.N. Cantwell, M. P. Lin, J.C. Price, Comparative evaluation of MR-based partial-volume correction schemes for PET, J. Nucl. Med. (1999).

[15] H.W. Müller-Gärtner, J.M. Links, J.L. Prince, R.N. Bryan, E. McVeigh, J.P. Leal, C. Davatzikos, J.J. Frost, Measurement of radiotracer concentration in brain gray matter using positron emission tomography: MRI-based correction for partial volume effects, J. Cereb. Blood Flow Metab. (1992), https://doi.org/10.1038/jcbfm.1992.81.

[16] M. Sattarivand, M. Kusano, I. Poon, C. Caldwell, Symmetric geometric transfer matrix partial volume correction for PET imaging: Principle, validation and robustness, Phys. Med. Biol. (2012), https://doi.org/10.1088/0031-9155/57/21/7101.

[17] C. Marini, S. Morbelli, A. Cistaro, C. Campi, C. Caponnetto, M. Bauckneht, A. Bellini, A. Buschiazzo, I. Calamia, M.C. Beltrametti, S. Margotti, P. Fania, I. Poggi, C. Cabona, S. Capitanio, R. Piva, A. Calvo, C. Moglia, A. Canosa, A. M. Massone, G. Nobili, F. Mancardi, A. Chio, M. Piana, G. Sambuceti, Interplay between spinal cord and cerebral cortex metabolism in amyotrophic lateral sclerosis, Brain (2018), https://doi.org/10.1093/brain/awy152.

[18] H. Endo, K. Sekiguchi, T. Ueda, H. Kowa, F. Kanda, T. Toda, Regional glucose hypometabolic spread within the primary motor cortex is associated with amyotrophic lateral sclerosis disease progression: A fluoro-deoxyglucose positron emission tomography study, ENeurologicalSci (2017), https://doi.org/10.1016/j.ensci.2017.01.001.

[19] M. Pagani, A. Chiò, M.C. Valentini, J. Öberg, F. Nobili, A. Calvo, C. Moglia, D. Bertuzzo, S. Morbelli, F. De Carli, P. Fania, A. Cistaro, Functional pattern of brain FDG-PET in amyotrophic lateral sclerosis, Neurology (2014), https://doi.org/10.1212/WNL.0000000000000792.

[20] A. Cistaro, M.C. Valentini, A. Chiò, F. Nobili, A. Calvo, C. Moglia, A. Montuschi, S. Morbelli, D. Salmaso, P. Fania, G. Carrara, M. Pagani, Brain hypermetabolism in amyotrophic lateral sclerosis: A FDG PET study in ALS of spinal and bulbar onset, Eur. J. Nucl. Med. Mol. Imaging (2012), https://doi.org/10.1007/s00259-011-1979-6.

[21] M.S. Buhour, F. Doidy, A. Mondou, A. Pélerin, L. Carluer, F. Eustache, F. Viader, B. Desgranges, Voxel-based mapping of grey matter volume and glucose metabolism profiles in amyotrophic lateral sclerosis, EJNMMI Res. (2017), https://doi.org/10.1186/s13550-017-0267-2.

[22] B.R. Brooks, R.G. Miller, M. Swash, T.L. Munsat, El Escorial revisited: Revised criteria for the diagnosis of amyotrophic lateral sclerosis, Amyotroph. Lateral Scler (2000), https://doi.org/10.1080/146608200300079536.

[23] J.M. Cedarbaum, N. Stambler, E. Malta, C. Fuller, D. Hilt, B. Thurmond, A. Nakanishi, The ALSFRS-R: a revised ALS functional rating scale that incorporates assessments of respiratory function. BDNF ALS Study Group (Phase III), J. Neurol. Sci. (1999).

[24] A.M. Dale, B. Fischl, M.I. Sereno, Cortical surface-based analysis: I. Segmentation and surface reconstruction, Neuroimage (1999), https://doi.org/10.1006/nimg.1998.0395.

[25] D.N. Greve, C. Svarer, P.M. Fisher, L. Feng, A.E. Hansen, W. Baare, B. Rosen, B. Fischl, G.M. Knudsen, Cortical surface-based analysis reduces bias and variance in kinetic modeling of brain PET data, Neuroimage (2014), https://doi.org/10.1016/j.neuroimage.2013.12.021.

[26] K. Erlandsson, I. Buvat, P.H. Pretorius, B.A. Thomas, B.F. Hutton, A review of partial volume correction techniques for emission tomography and their applications in neurology, cardiology and oncology, Phys. Med. Biol. (2012), https://doi.org/10.1088/0031-9155/57/21/R119.

[27] T.W. Chow, M.A. Binns, M. Freedman, D.T. Stuss, J. Ramirez, C.J.M. Scott, S. Black, Overlap in frontotemporal atrophy between normal aging and patients with frontotemporal dementias, Alzheimer Dis. Assoc. Disord. (2008), https://doi.org/10.1097/WAD.0b013e31818026c4.

[28] P.M. Ferraro, C. Cabona, G. Meo, C. Rolla-Bigliani, L. Castellan, M. Pardini, M. Inglese, C. Caponnetto, L. Roccatagliata, Age at symptom onset influences cortical thinning distribution and survival in amyotrophic lateral sclerosis, Neuroradiology (2021), https://doi.org/10.1007/s00234-021-02681-3.

[29] R.A.L. Menke, M. Proudfoot, K. Talbot, M.R. Turner, The two-year progression of structural and functional cerebral MRI in amyotrophic lateral sclerosis, NeuroImage Clin. (2018), https://doi.org/10.1016/j.nicl.2017.12.025.

[30] C. Schuster, E. Kasper, J. Machts, D. Bittner, J. Kaufmann, R. Benecke, S. Teipel, S. Vielhaber, J. Prudlo, Longitudinal course of cortical thickness decline in amyotrophic lateral sclerosis, J. Neurol. (2014), https://doi.org/10.1007/s00415-014-7426-4.

[31] F. Trojsi, F. Di Nardo, M. Siciliano, G. Caiazzo, C. Femiano, C. Passaniti, D. Ricciardi, A. Russo, A. Bisecco, S. Esposito, M.R. Monsurrò, M. Cirillo, G. Santangelo, F. Esposito, G. Tedeschi, Frontotemporal degeneration in amyotrophic lateral sclerosis (ALS): A longitudinal MRI one-year study, CNS Spectr. (2020), https://doi.org/10.1017/S109285292000005X.

[32] P.M. Ferraro, C. Jester, C.A. Olm, K. Placek, F. Agosta, L. Elman, L. McCluskey, D. J. Irwin, J.A. Detre, M. Filippi, M. Grossman, C.T. McMillan, Perfusion alterations converge with patterns of pathological spread in transactive response DNA-binding protein 43 proteinopathies, Neurobiol. Aging. (2018), https://doi.org/10.1016/j.neurobiolaging.2018.04.008.

[33] H.K. van der Burgh, H.J. Westeneng, R. Walhout, K. van Veenhuijzen, H.H.G. Tan, J.M. Meier, L.A. Bakker, J. Hendrikse, M.A. van Es, J.H. Veldink, M.P. van den Heuvel, L.H. van den Berg, Multimodal longitudinal study of structural brain involvement in amyotrophic lateral sclerosis, Neurology (2020), https://doi.org/10.1212/WNL.0000000000009498.

[34] Y.J. Jeong, H.J. Yoon, D.Y. Kang, Assessment of change in glucose metabolism in white matter of amyloid-positive patients with Alzheimer disease using F-18 FDG PET, Med. (United States). (2017), https://doi.org/10.1097/MD.0000000000009042.

[35] K.T. Oh, D. Kim, B.S. Ye, S. Lee, M. Yun, S.K. Yoo, Segmentation of white matter hyperintensities on 18F-FDG PET/CT images with a generative adversarial network, Eur. J. Nucl. Med. Mol. Imaging. (2021), https://doi.org/10.1007/s00259-021-05285-4.

[36] C. Coello, F. Willoch, P. Selnes, L. Gjerstad, T. Fladby, A. Skretting, Correction of partial volume effect in 18F-FDG PET brain studies using coregistered MR volumes: Voxel based analysis of tracer uptake in the white matter, Neuroimage (2013), https://doi.org/10.1016/j.neuroimage.2013.01.043.